Electronic Supplementary Information for

Single Crystals of Organometallic Manganese Halides as Sustainable High-Luminescence Materials for X-ray Scintillation

Azimet A. Karluk,[a,b,c] Simil Thomas,[b] Aleksander Shkurenko,[b] Bashir E. Hasanov,[c] Javeed Mahmood,[*a,b,c] Mohamed Eddaoudi,[*b] and Cafer T. Yavuz[*a,b,c]

[a]Oxide & Organic Nanomaterials for Energy & Environment (ONE) Laboratory, Physical Science & Engineering (PSE), King Abdullah University of Science and Technology (KAUST), Thuwal 23955, Saudi Arabia

[b]Advanced Membranes & Porous Materials (AMPM) Center, Physical Science & Engineering (PSE), King Abdullah University of Science and Technology (KAUST), Thuwal 23955, Saudi Arabia

[c]KAUST Catalysis Center (KCC), Physical Science & Engineering (PSE), King Abdullah University of Science and Technology (KAUST), Thuwal 23955, Saudi Arabia.

*Correspondence: cafer.yavuz@kaust.edu.sa (C.T.Y), mohamed.eddaoudi@kaust.edu.sa (M.E.), javeed.mahmood@kaust.edu.sa (J.M.)

Table S1. Single crystal X-ray diffraction data and structure refinement of $(MTP)_2MnCl_4$

Empirical formula	$C_{38}H_{36}Cl_{4.07}MnP_2$
Formula weight	753.65
Crystal system, space group	Cubic, $P2_13$
Unit cell dimensions	a = 15.4331(2) Å
Volume	3675.9(1) Å^3
Z, calculated density	4, 1.362 Mg m^{-3}
F(000)	1552
Temperature (K)	120.0(1)
Radiation type, λ	Cu $K\alpha$, 1.54178 Å
Absorption coefficient	6.66 mm^{-1}
Absorption correction	Multi-scan
Max and min transmission	0.156 and 0.051
Crystal size	0.010 × 0.013 × 0.017 mm
Shape, colour	Tetrahedron, pale green
θ range for data collection	4.0–72.4°
Limiting indices	$-14 \le h \le 19$, $-17 \le k \le 13$, $-17 \le l \le 13$
Reflection collected / unique / observed with $I > 2\sigma(I)$	14212 / 2397 (R_{int} = 0.058) / 2246
Completeness to θ_{full} = 67.6°	99.6 %
Refinement method	Full-matrix least-squares on F^2
Data / restraints / parameters	2397 / 0 / 118
Final R indices [$I > 2\sigma(I)$]	R_1 = 0.035, wR_2 = 0.079
Final R indices (all data)	R_1 = 0.039, wR_2 = 0.085
Weighting *scheme*	$[\sigma^2(F_o^2) + (0.0555P)^2 + 0.5433P]^{-1}$*
Goodness-of-fit	1.01
Flack parameter	-0.004(4)
Largest diff. peak and hole	0.43 and -0.23 e Å^{-3}

Table S2. Single crystal X-ray diffraction data and structure refinement of $(PTA)_2MnCl_4$

Empirical formula	$C_{18}H_{28}Cl_4MnN_2$
Formula weight	469.16
Crystal system, space group	Monoclinic, *C*2/*c*
Unit cell dimensions	a = 15.6013(7) Å
	b = 9.5377(7) Å, β = 95.293(3)°
	c = 30.841(2) Å
Volume	4569.6(5) Å^3
Z, calculated density	8, 1.364 Mg m^{-3}
F(000)	1944
Temperature (K)	200.0(1)
Radiation type, λ	Mo *K*α, 0.71073 Å
Absorption coefficient	1.05 mm^{-1}
Absorption correction	Multi-scan
Max and min transmission	0.745 and 0.664
Crystal size	0.01 × 0.01 × 0.01 mm
Shape, colour	Prism, pale green
θ range for data collection	2.5–23.3°
Limiting indices	$-17 \le h \le 17$, $-10 \le k \le 10$, $-34 \le l \le 34$
Reflection collected / unique / observed with $I > 2\sigma(I)$	33000 / 3259 (R_{int} = 0.019) / 3155
Completeness to θ_{full} = 23.3°	99.1 %
Refinement method	Full-matrix least-squares on F^2
Data / restraints / parameters	3259 / 136 / 302
Final *R* indices [$I > 2\sigma(I)$]	R_1 = 0.023, wR_2 = 0.057
Final *R* indices (all data)	R_1 = 0.024, wR_2 = 0.058
Weighting *scheme*	$[\sigma^2(F_o^2) + (0.0206P)^2 + 5.3513P]^{-1}$*
Goodness-of-fit	1.19
Largest diff. peak and hole	0.25 and -0.18 e Å^{-3}

*$P = (F_o^2 + 2F_c^2)/3$

Note: Single Crystal X-Ray Diffraction Study of $(MTP)_2MnCl_4$ and $(PTA)_2MnCl_4$

There is an occupational disorder in the structure of $(MTP)_2MnCl_4$: in 93.5% of the $MnCl_4$ entity, the metal cation is Mn(II), and in the remaining 6.5%, Mn(III) is present. This results in a lower charge of the $MnCl_4$ entity ($[Mn(II)Cl_4]^{2-}$ vs $[Mn(III)Cl_4]^{-}$). Therefore, the two $(MTP)^+$ cations are additionally balanced by chloride Cl^- anion with an occupancy of 6.5%. In $(PTA)_2MnCl_4$, one of the two crystallographically independent phenyltrimethylammonium cations (PTA) is significantly disordered with the occupancies of 58% and 42% for the parts A and B, respectively. Therefore, the C–N bond lengths were restrained to be the same by the SADI. The ADPs of the organic cations were restrained to be similar by strong SIMU. Benzene ring geometries in all three structures were constrained by AFIX 66. Hydrogen atoms of the organic ligands were placed at the calculated positions and refined using a riding model with Uiso(H) = 1.2Ueq(Csp2) or 1.5Ueq(Csp3).

The X-ray crystallographic data for $(MTP)_2MnCl_4$ and $(PTA)_2MnCl_4$ have been deposited at the Cambridge Crystallographic Data Centre (CCDC), under deposition numbers 2353441-2353443. These data can be obtained free of charge from the CCDC via www.ccdc.cam.ac.uk.

Experimental Section

Chemicals. Methyltriphenylphosphonium chloride (MTPCl, >97.0%) and poly (methyl methacrylate) (PMMA, average Mw ~350,000) were purchased from Sigma-Aldrich. Phenyltrimethylammonium chloride (PTACl, 99.99%) was purchased from Alfa Aesar, Manganese chloride tetrahydrate ($MnCl_2.4H_2O$, ≥99.95%), dichloromethane (DCM, 99.9%), diethyl ether (99.8%), and ethyl acetate were purchased from VWR. All the chemicals were used as received without further purification.

Growth of $(MTP)_2MnCl_4$ Crystals: To grow 0D $(MTP)_2MnCl_4$ crystals, a solution was prepared by dissolving $MnCl_2$ (125.84 mg, 1.0 mmol) and MTPCl (625.54 mg, 2.0 mmol) in 4 mL of DCM (dichloromethane). The solution was then filtered using a 0.22 μm filter into a 5 mL vial. Next, the vial containing the filtered solution was placed inside a 20 mL vial filled with 10 mL of diethyl ether. The entire setup was sealed and left undisturbed overnight, resulting in the formation of greenish blocks of crystals.

Growth of $(PTA)_2MnCl_4$ Crystals: To grow 0D $(PTA)_2MnCl_4$ crystals, a solution was prepared by dissolving $MnCl_2$ (125.84 mg, 1.0 mmol) and PTACl (343.34 mg, 2.0 mmol) in 5 mL of deionized water. The solution was stirred for 2 h until it became a clear solution and then filtered using a 0.22 μm filter into a 10 mL vial. The vial containing the filtered solution was placed at 75 °C and sealed with aluminum foil with tiny holes. It was left undisturbed overnight, resulting in the formation of greenish block crystals.

To fabricate $(MTP)_2MnCl_4$ powders and films, $(MTP)_2MnCl_4$ crystals were ground manually using a pestle for 40 minutes to obtain the powders. Next, 1 g of PMMA was dissolved in 10 ml of ethyl acetate and stirred for 3 h until it was fully dissolved. Subsequently, 100 mg of $(MTP)_2MnCl_4$

powder was dispersed in a small amount of ethyl acetate and sonicated for 30 min. The dispersed powder was slowly added to the PMMA solution and stirred for 10 h. Finally, the PMMA+ $(MTP)_2MnCl_4$ mixture was poured slowly into a glass Petri dish and left undisturbed overnight for solidification.

Characterization.

The X-ray diffraction patterns were collected using a Bruker D8 ADVANCE diffractometer with Cu Kα radiation (λ = 1.5406 Å) at a scan rate of 1°/min. Single Crystal X-ray Diffraction data were collected using Bruker D8 Venture Photon100 diffractometer using either CuKα (λ = 1.54178 Å) for $(MTP)_2MnCl_4$ or MoKα radiation (λ = 0.71073 Å) for $(PTA)_2MnCl_4$. Indexing was performed using APEX3 v2018.7-2 (Difference Vectors method). Data integration and reduction were performed using SaintPlus 8.38A. Absorption correction was performed by multi-scan method implemented in SADABS-2016/2. Space group was determined using XPREP implemented in APEX3. The structure was solved using Direct Methods (SHELXS-2008) and refined using SHELXL-2019/2 (full-matrix least-squares on F^2) contained OLEX2 program package. SEM and EDX analyses were performed using a Carl Zeiss Merlin high-resolution scanning electron microscope equipped with an EDX detector. Steady-state Photoluminescence spectra were recorded using a Horiba Fluoromax-4 spectrofluorometer equipped with a photomultiplier (PMT-928). Photoluminescence quantum yields were obtained using an Edinburgh Instruments FLS920 Fluorescence Spectrometer equipped with a 450 W continuous wavelength xenon lamp and an integrating sphere. Time-resolved photoluminescence measurements were performed using the Time-Correlated Single-Photon counting technique (TCSPC). The excitation wavelength (320 nm) was adjusted using a parametric optical amplifier (Newport, Spectra-Physics) pumped with an Astrella femtosecond pulsed laser (Coherent). The energy at each excitation

wavelength was set to a constant (34 nJ) using variable neutral density filters (Thorlabs). The beam was directed into a Halcyone setup (Ultrafast Systems), focused on the sample, and the photoluminescence was collected and recollimated by a pair of parabolic mirrors, passed through a long-pass filter (520 nm, Newport), and focused on the monochromator and detector. The TCSPC histograms were fitted using the Lavenberg-Marquart algorithm implemented in Ultrafast System software. The overall time resolution of the system was greater than 120 ps. Temperature-dependent photoluminescence (PL) spectra were recorded. The excitation laser was a 325 nm UV laser. A grating with 300 grooves/mm was used for all measurements. The integration time was 1s for $(MTP)_2MnCl_4$ and $(PTA)_2MnCl_4$ since these two samples have relatively low PL intensity. The number of accumulations was maintained at 20 °C for all the measurements. The temperature was controlled by a Linkam THMS600 stage from -195 °C to 225 °C at 20 °C intervals. A Thorlabs 15x UV objective lens was used for all the measurements. Thermogravimetric analysis (TGA) was performed on a TGA-TA Discovery 5500 instrument. The heating rates for all samples were set as 10 °C min^{-1} under nitrogen flow. The UV–vis spectra and transmittance spectra were recorded using a Lambda 950 spectrophotometer equipped with an integrating sphere, acquired from 200 to 2500nm.

The Radioluminescence (RL) spectra were acquired using a Horiba Fluromax-4 spectrometer equipped with a tungsten target X-ray tube (Moxtek). For all spectral measurements, the detection slit was set at 5 nm and the X-ray outlet was positioned 1 cm away from the sample. The X-ray dose rate varied between 3.43 μGy/s to 31.63 mGy/s by controlling the input current and voltage values. All the experiments were performed in a radiation-tight environment shielded by lead plates.

The light yields of the film samples were estimated using a commercial BGO scintillator. We prepared a tablet (using a manual hydraulic press) from a powder with a thickness similar to that

of the BGO standard (~0.5 mm), and RL curves were acquired using the spectrometer under identical experimental conditions. To validate the accuracy of this method, a LYSO: Ce scintillator was also employed as a reference. Temperature-dependent radioluminescence measurements were conducted over a temperature range of 150 K to 425 K, with each temperature maintained for 10 minutes. The X-ray tube was operated at a voltage of 50 kV and a current of 50 μA, with the detection slit of 1 nm.

X-ray Imaging Data Acquisition and Processing. To capture images of the flexible large-area X-ray imaging film, a commercial camera (D7100, Nikon) was employed. For samples excited by X-rays, the ISO, aperture, and shutter were set to 600, F3.2, and 15, respectively. High-resolution X-ray imaging was conducted using an inverted fluorescence microscope (Axio Vert. A1, Carl Zeiss) coupled with a portable X-ray tube (tungsten target; Moxtek). The X-ray tube's voltage/current was set to 50 kV/100μA under an objective lens of varying magnifications at 5 ×. The X-ray images were collected using a camera (DS-Ri1, Nikon) with an exposure time of 30 s. The resulting X-ray images were subsequently processed using ImageJ software to eliminate the screen background.

Computational Method

Density functional theory (DFT) calculations were performed using the projector-augmented wave (PAW) method implemented in the Vienna *ab-initio* simulation package (VASP)[1, 2] within the generalized gradient approximation (GGA) using the Perdew, Burke, and Ernzerhof (PBE) exchange–correlation functional. PBE+U method following the approach of Dudarev[3] was used to account for the strong on-site Coulomb repulsion amongst the localized Mn 3d electrons, and the Grimme semi-empirical D3 dispersion method[4] with the Becke-Johnson damping[5] was included to model to account for the long-range dispersion interactions. In the GGA+U calculations, we used

the U values (U = 4.0 eV) derived in a previous study for Mn 3d electrons[6]. The kinetic energy cut-off was fixed at 400 eV for the plane-wave basis and a dense, Γ-point-centered, Monkhorst-Pack k-point mesh (spacing ≤0.03 Å−1)[7] to sample the Brillouin zone. The crystal structure was relaxed until the atomic force was less than 0.02 eV/Å.

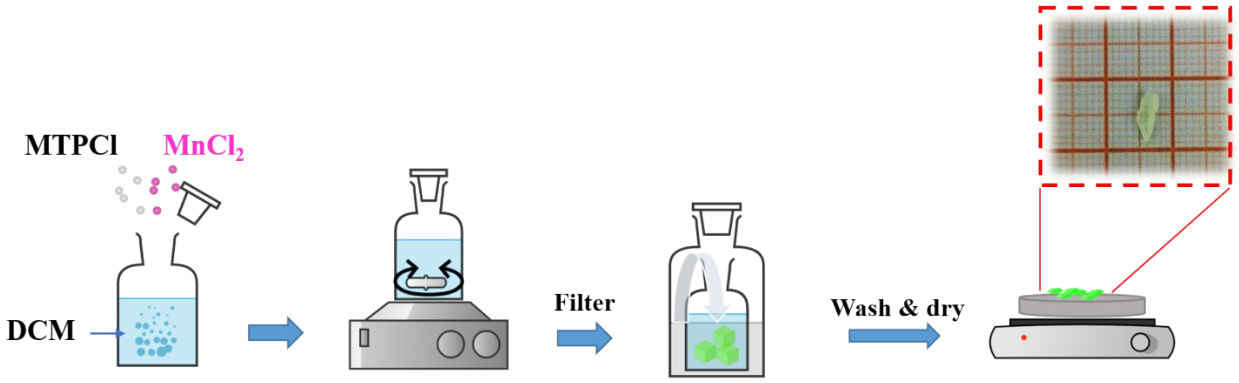

Figure S1. Crystal growth process of $(MTP)_2MnCl_4$.

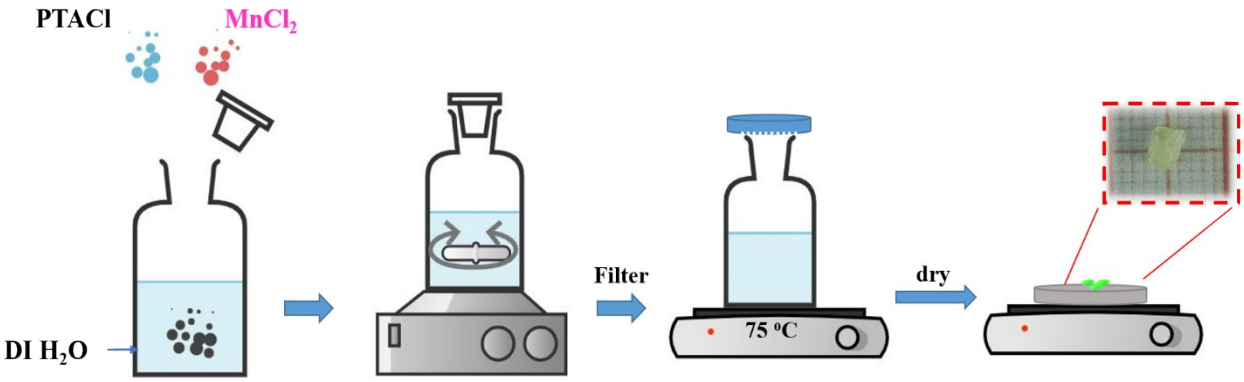

Figure S2. Crystal growth process of $(PTA)_2MnCl_4$

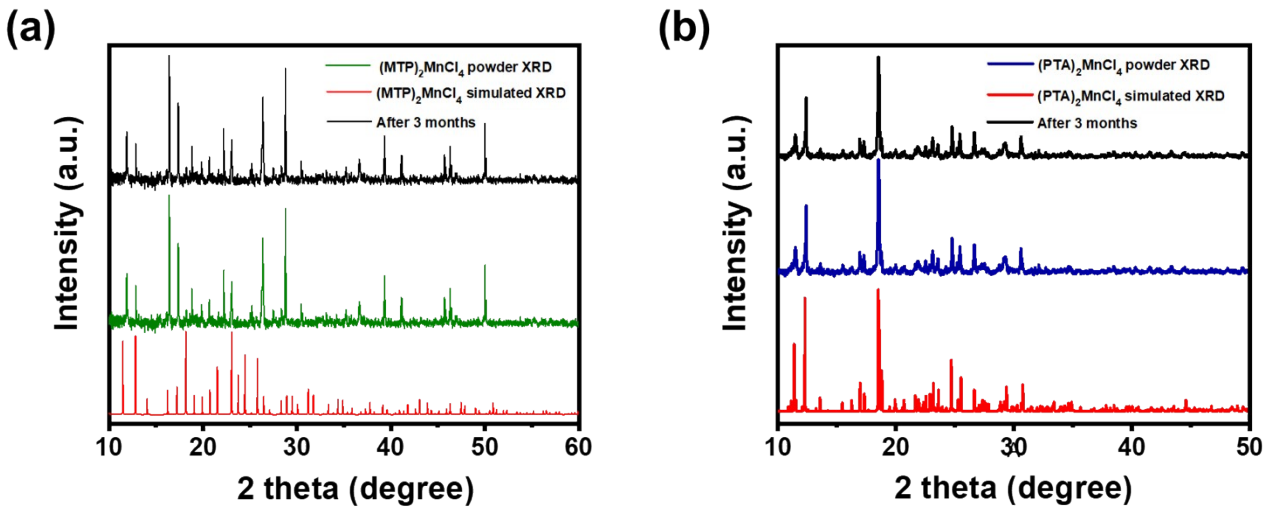

Figure S3. PXRD patterns of (**a**) $(MTP)_2MnCl_4$ and (**b**) $(PTA)_2MnCl_4$: as-synthesized, exposed to air for three months and the XRD patterns derived from SCXRD refinement.

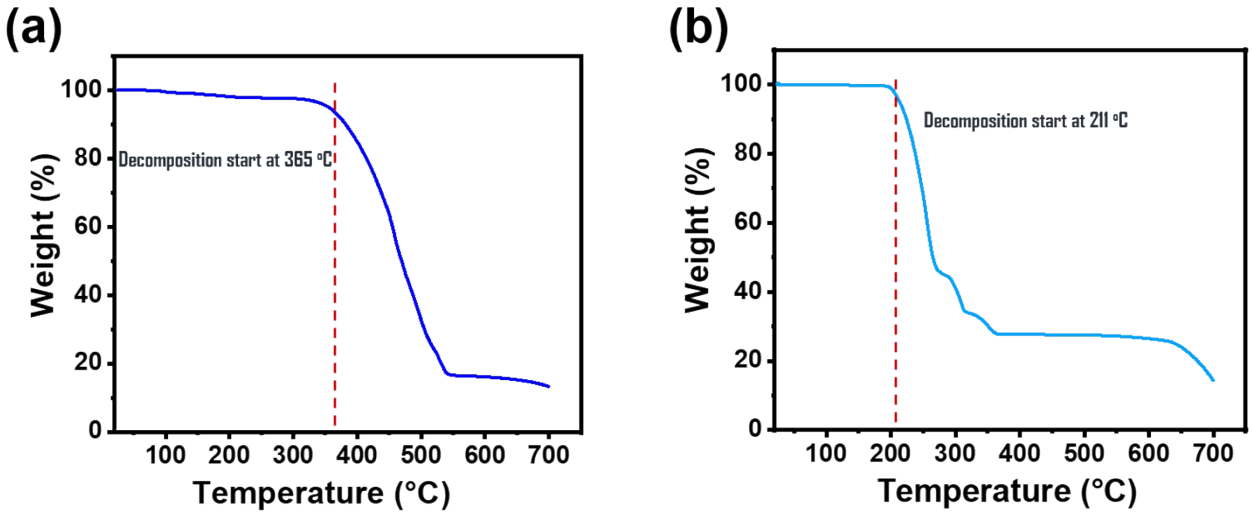

Figure S4. TGA curves of (**a**) $(MTP)_2MnCl_4$ and (**b**) $(PTA)_2MnCl_4$.

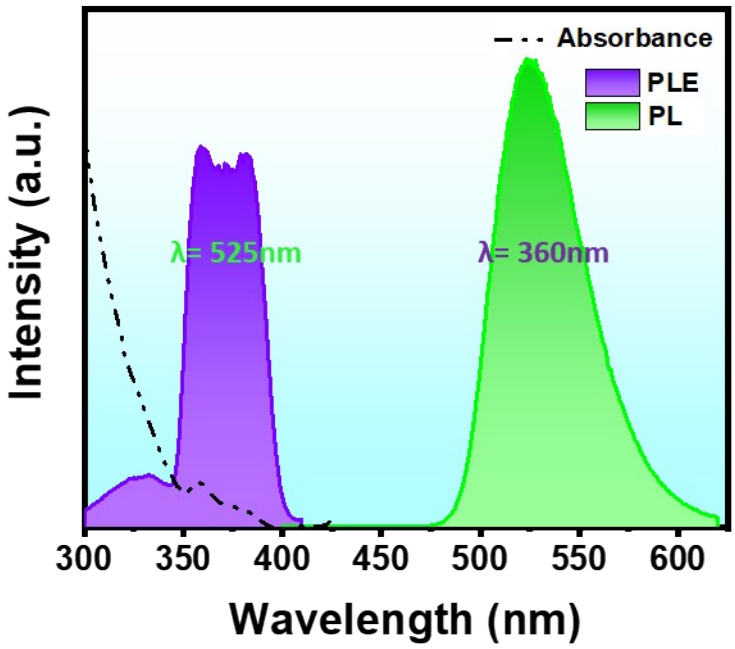

Figure S5. Solid-state UV−Vis absorption spectrum, PL excitation and emission Spectra of $(PTA)_2MnCl_4$.

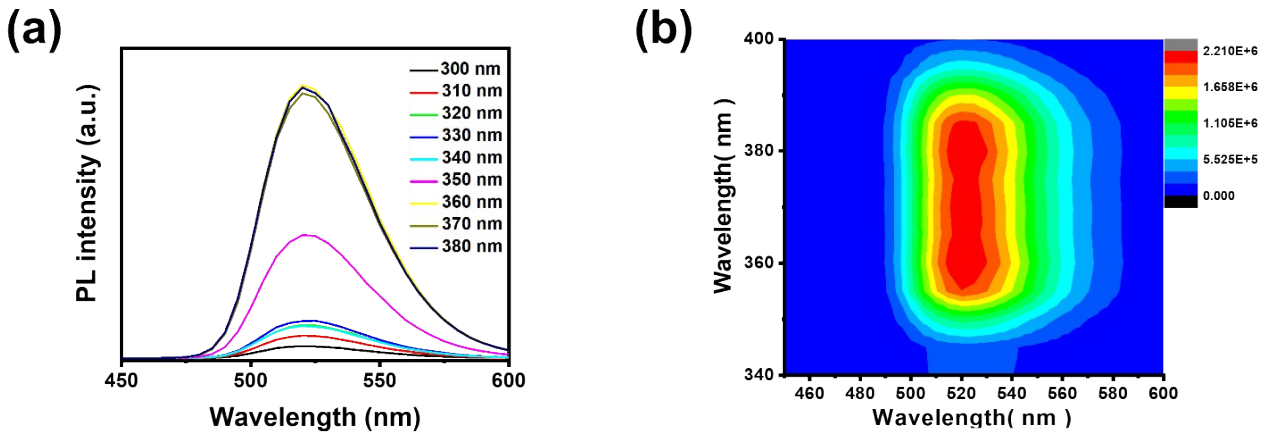

Figure S6. Excitation wavelength (300−380 nm) dependent PL emission spectra (**a**), Color mapping of the consecutive 3D PL spectrum of $(PTA)_2MnCl_4$ (**b**).

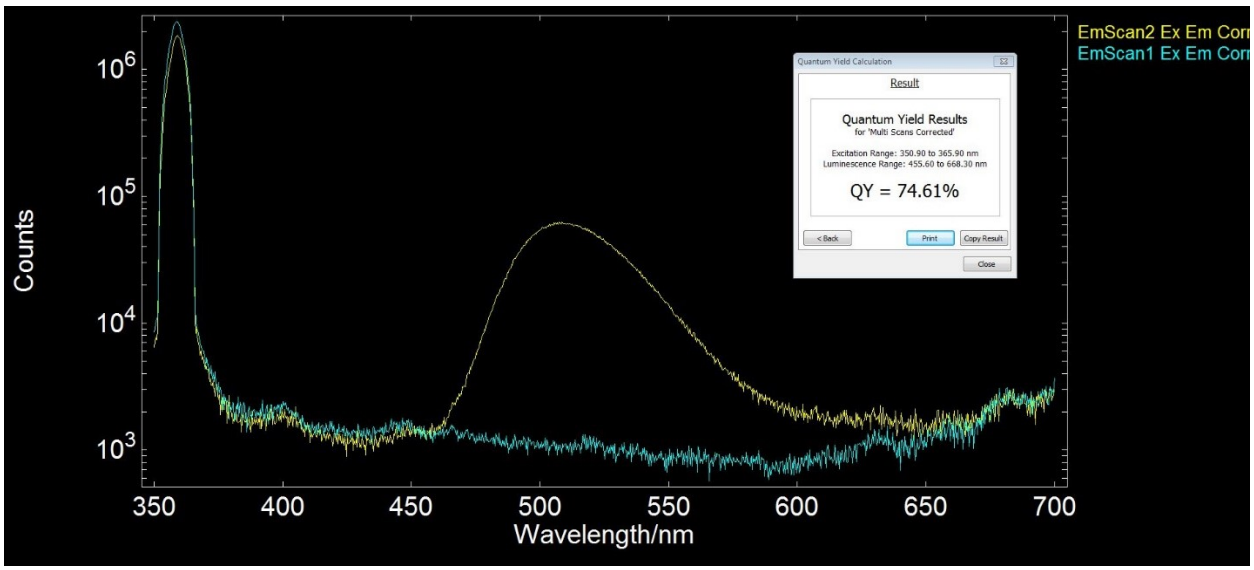

Figure S7. PLQY of $(MTP)_2MnCl_4$ crystal.

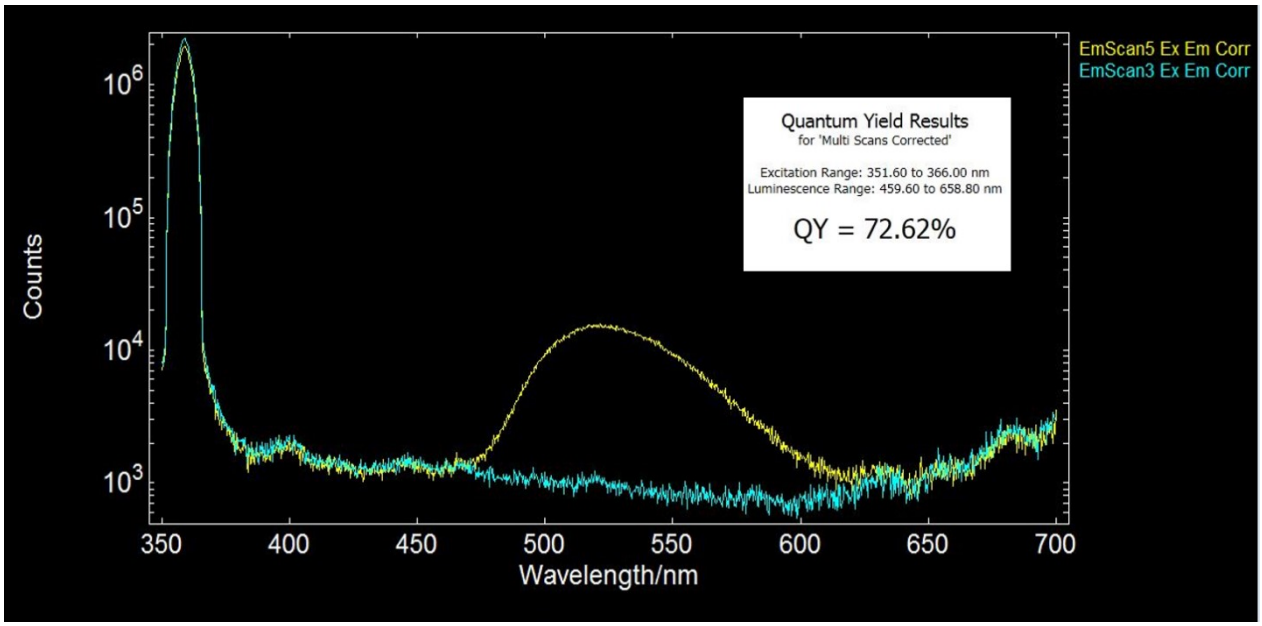

Figure S8. PLQY of $(PTA)_2MnCl_4$ crystal.

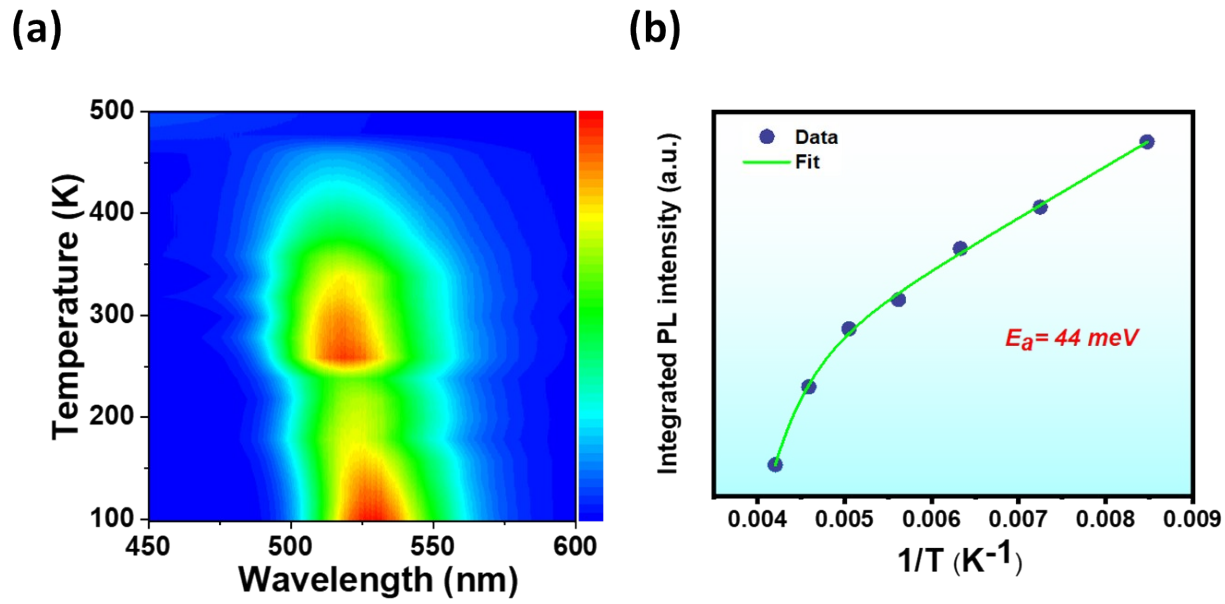

Figure S9. (**a**) Color mapping of temperature-dependent PL emission spectra and (**b**) experimental and fitted emission intensity vs. temperature of $(PTA)_2MnCl_4$.

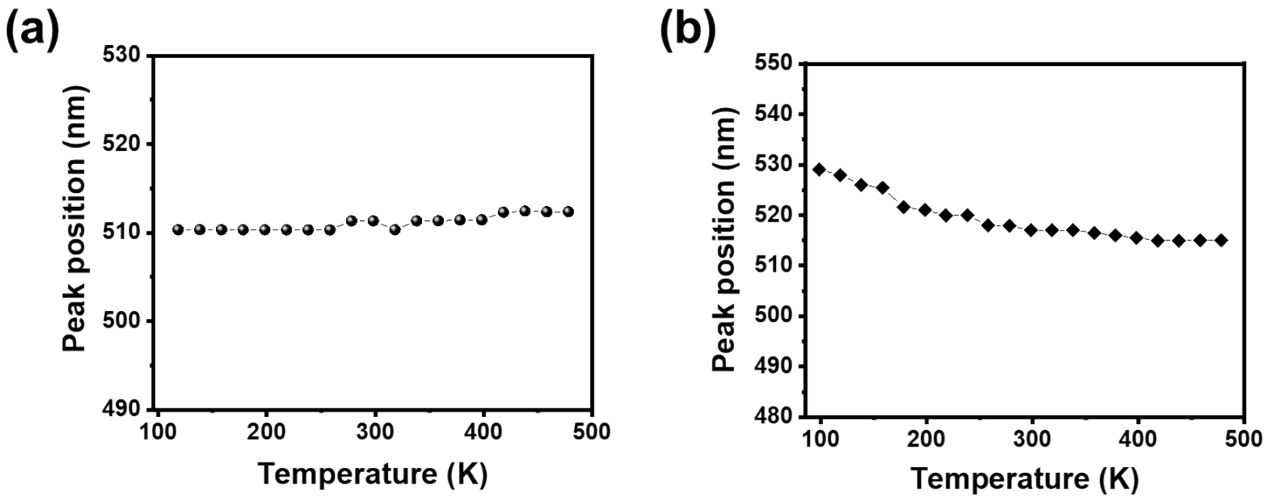

Figure S10. PL peak position as a function of temperature of (a) $(MTP)_2MnCl_4$ (b) $(PTA)_2MnCl_4$.

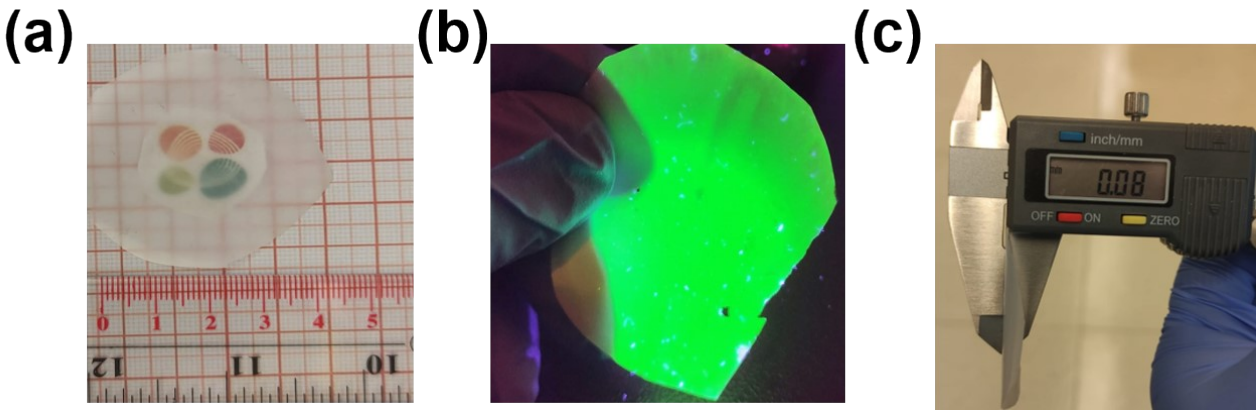

Figure S11. Photographs of the $(MTP)_2MnCl_4$-PMMA composite film were taken under ambient light (**a**) and UV light (**b**). The thickness of the film was measured using a Vernier caliper (**c**).

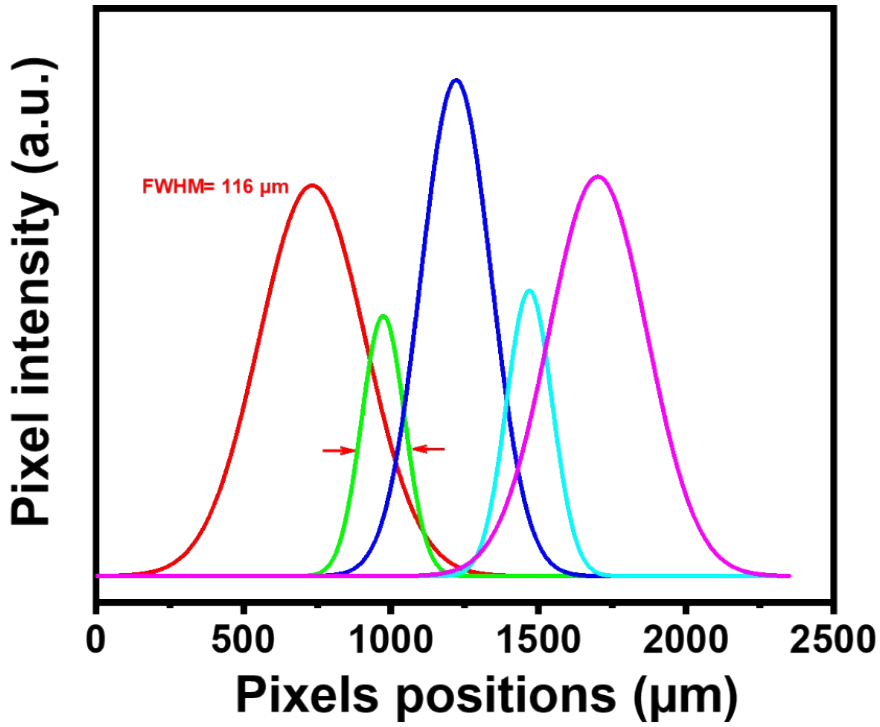

Figure S12. Spatial resolution was obtained by fitting the intensity spread profile of the crystalline scintillation screen with a Gaussian function.

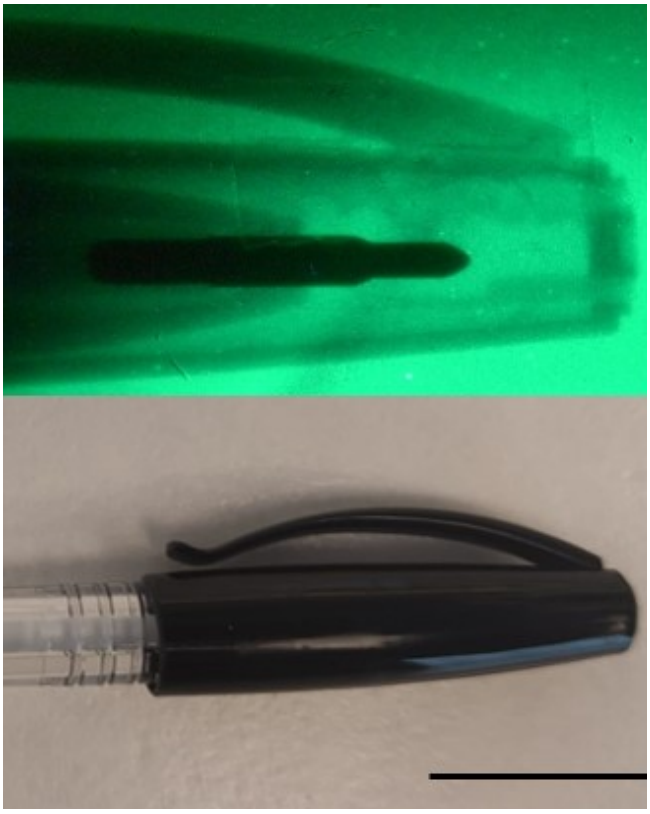

Figure S13. Clear recognition of the metal part of a ballpoint pen, under X-ray irradiation (50 kV, 100 μA) Scale bar: 1 cm.

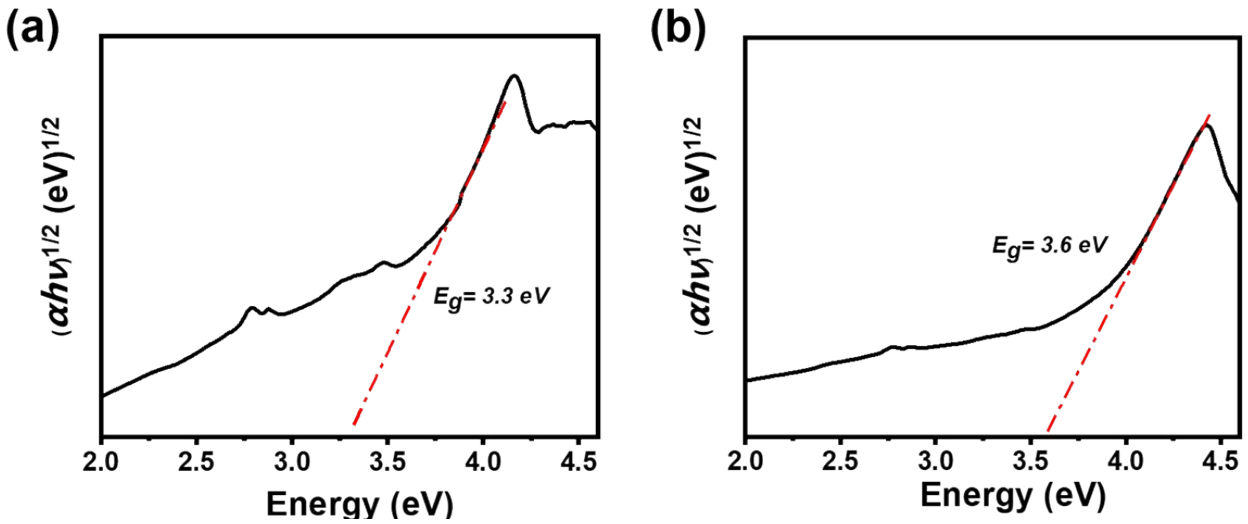

Figure S14. Tauc plot of (**a**) $(MTP)_2MnCl_4$ and (**b**) $(PTA)_2MnCl_4$.

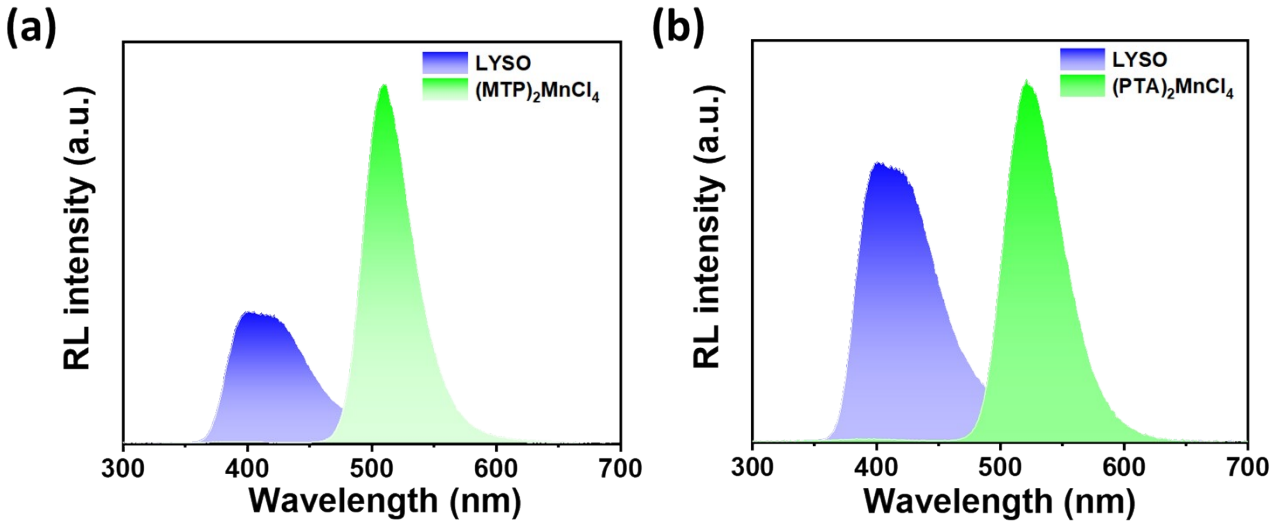

Figure S15. X-ray excited radioluminescence (RL) spectra of crystals 1, 2 and LYSO under 30 kV and 30 μA X-ray excitation.

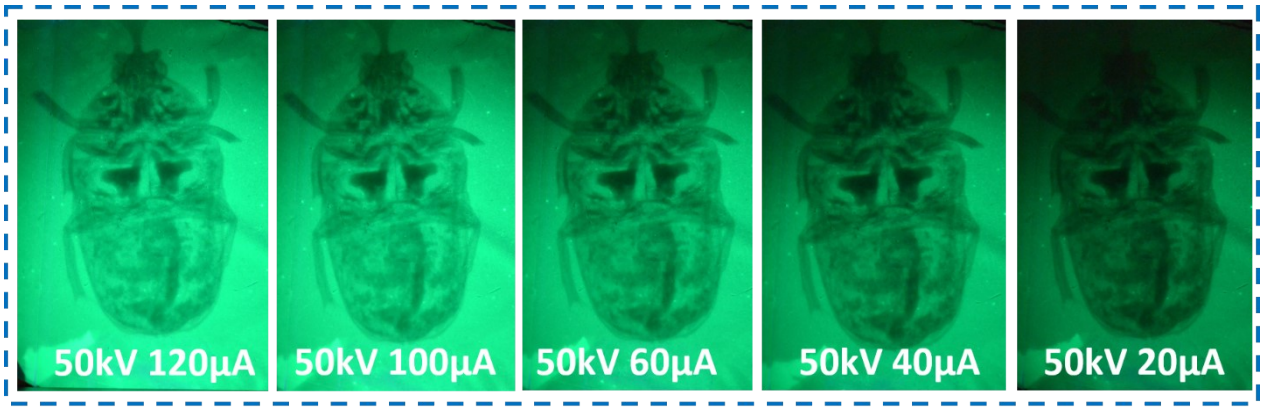

Figure S16. X-ray imaging of Scarab beetle under different X-ray power ranging from 50kV 20 μA to 120 μA.

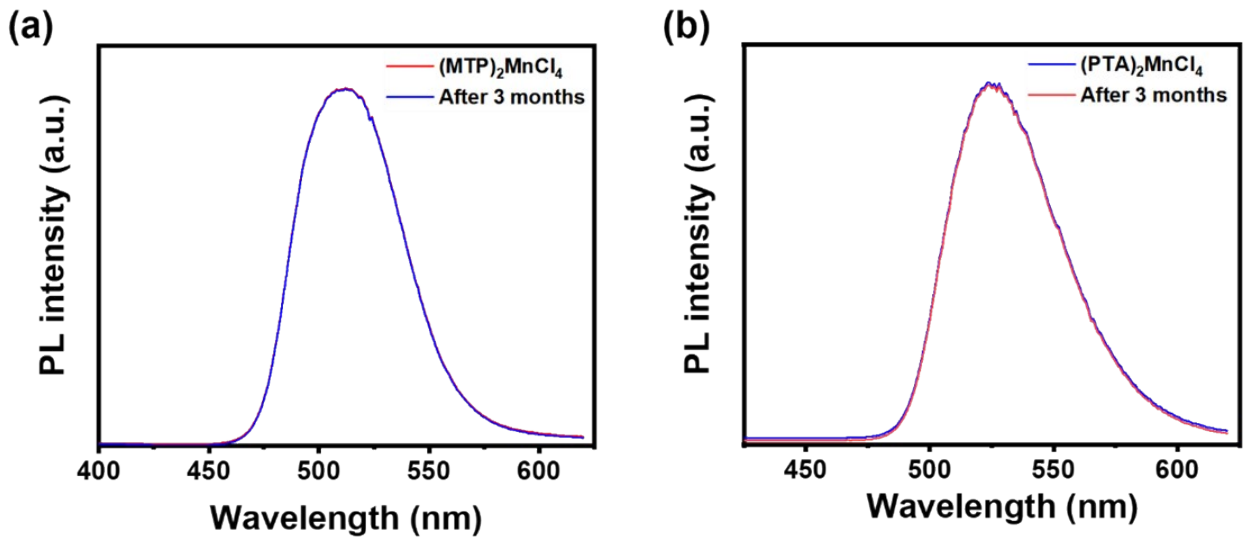

Figure S17. PL spectra of (**a**) $(MTP)_2MnCl_4$ and (**b**) $(PTA)_2MnCl_4$: as-synthesized, exposed to air for three months.

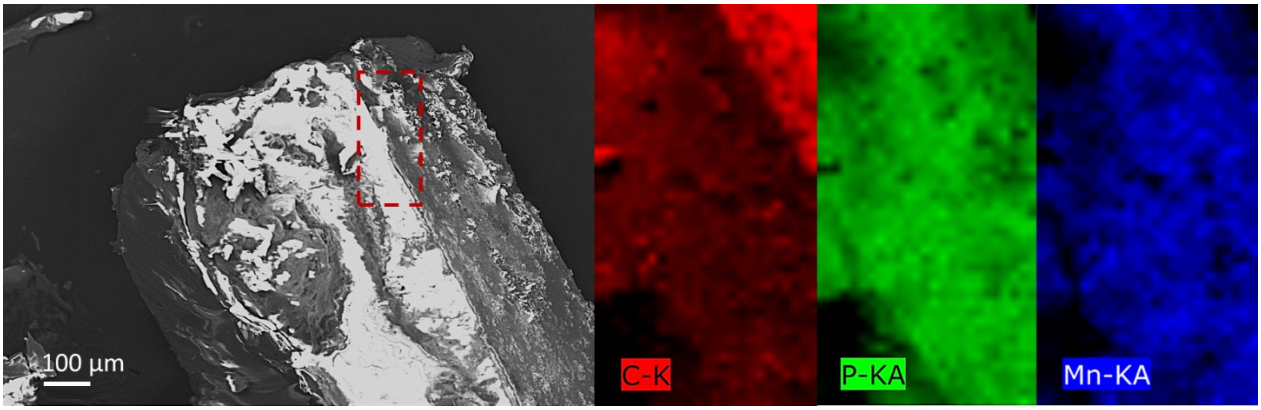

Figure S18. SEM and EDS mapping of $(MTP)_2MnCl_4$ crystal.

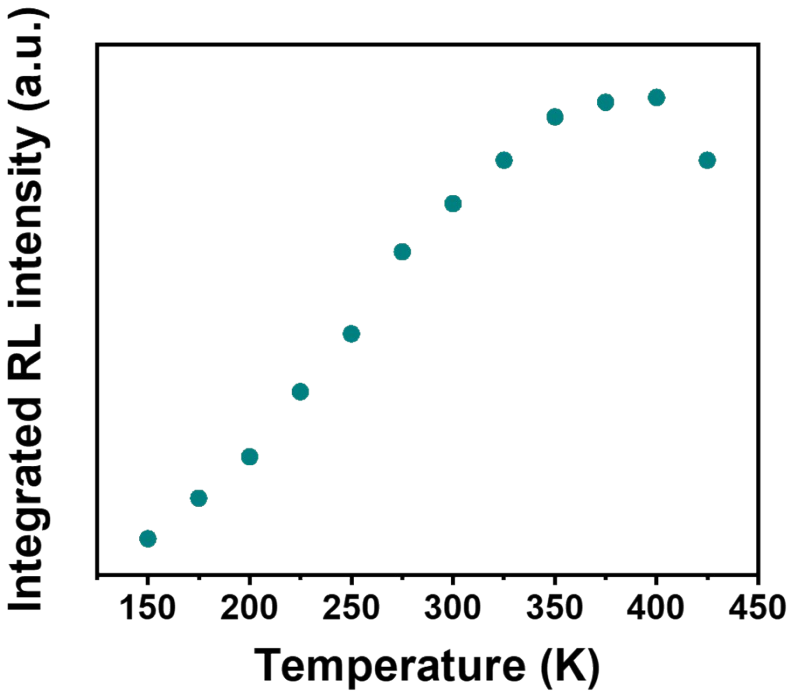

Figure S19. Temperature dependent RL emission of the $(MTP)_2MnCl_4$ crystal.

References

1. G. Kresse and J. Hafner, *Phys. Rev. B*, 1993, **48**, 13115.
2. G. Kresse and J. Furthmüller, *Phys. Rev. B* 1996, **54**, 11169.
3. S. L. Dudarev, G. A. Botton, S. Y. Savrasov, C. Humphreys and A. P. Sutton, *Phys. Rev. B* 1998, **57**, 1505.
4. S. Grimme, S. Ehrlich and L. Goerigk, *J. Comput. Chem.*, 2011, **32**, 1456-1465.
5. A. D. Becke and E. R. Johnson, *J. Chem. Phys.*, 2005, **123**.
6. B. Ramogayana, D. Santos-Carballal, P. A. Aparicio, M. G. Quesne, K. P. Maenetja, P. E. Ngoepe and N. H. de Leeuw, *PCCP*, 2020, **22**, 6763-6771.
7. V. Wang, N. Xu, J.-C. Liu, G. Tang and W.-T. Geng, *Comput. Phys. Commun.*, 2021, **267**, 108033.